Journal of
Materials Chemistry C

RSC Publishing

PAPER

View Article Online
View Journal | View Issue

Published on 30 October 2012. Downloaded by National Chiao Tung University on 28/04/2014 02:09:19.

Low operation voltage macromolecular composite memory assisted by graphene nanoflakes†

Cite this: J. Mater. Chem. C, 2013, 1, 552

Ying-Chih Lai,[a] Di-Yan Wang,[b] I-Sheng Huang,[b] Yu-Ting Chen,[c] Yung-Hsuan Hsu,[d] Tai-Yuan Lin,[e] Hsin-Fei Meng,[d] Ting-Chang Chang,[c] Ying-Jay Yang,[af] Chia-Chun Chen,[bg] Fang-Chi Hsu[h] and Yang-Fang Chen*[i]

Received 21st August 2012
Accepted 29th October 2012

DOI: 10.1039/c2tc00010e

www.rsc.org/materialsC

The trend towards simple and low-cost processing is one of the most important for macromolecular memory development. Here, bistable memory devices using a solution-processable active material, a mixture of graphene nanoflakes (GNFs) and insulating poly(vinyl alcohol) (PVA), are investigated, which serve as the first example for the direct integration of as-prepared nanoscale graphene into macromolecular memory devices through a one-step low-temperature processing method. Bistable electrical switching behavior and nonvolatile rewritable memory effects are realized by using an indium–tin-oxide/GNF–PVA/silver (ITO/GNF–PVA/Ag) sandwich structure. The resulting device exhibits low operation voltages of +1.4 V (turn-on) and −1.3 V (turn-off), which is promising for memory cells with low power consumptions. The programmable ON- and OFF-states possess a retention time of over 10^4 s and endure up to 10^7 read pulses. The carrier transport in the OFF- and ON-states follows the typical trap-limited space charge limited current and Ohmic laws, respectively. The asymmetric electrical switch behavior is therefore attributed to conducting filaments formed in the PVA layer assisted by the charged GNFs that induce the transition of the conductivity. Our study provides a potential approach for integrating as-prepared graphene into macromolecular memory devices with excellent performances through a simple solution-process.

Introduction

In the past few decades, various types of memory devices have been developed, such as ferroelectric random access memory devices,[1] phase-change random access memory devices,[2] resistance random access memory devices,[3] and so on.[4] Among them, macromolecular memory devices, also referred to as polymer or organic bistable devices, have attracted great attention from scientists as promising advanced nonvolatile memory devices[5,6] due to the following advantages: low-temperature simple processing, large-scale manufacturing, and simple device configuration.[7–9] The possibility of using organic materials in solution form results in a simple approach to deposition (*e.g.*, using a spin-coating method and ink-jet printing) which can be on a range of substrates such as plastic, glass, and rigid metal. Until now, several macromolecular memory systems have been developed such as functional polyimides,[10,11] organic donor–acceptor complexes,[12,13] and polymer–nanoparticle hybrids,[5,14] and other systems.[9,15] In particular, organic–inorganic composite memory systems have attracted great attention due to their high reproducibility, versatile composite materials, cost-effective spin-coating fabrication approach, and good device performance.[16]

Graphene, a two dimensional (2D) material with superior chemical and physical properties, has recently been studied progressively in the fields of condensed matter physics and material science. Due to its chemical stability,[17] high surface area,[7,18] excellent elasticity,[19,20] good transparency,[21] and high carrier mobility,[22,23] graphene has been incorporated into various technological applications. The successful use of graphene/graphene oxide as an active component in sensors,[24] field-effect transistors,[25–27] organic solar cells,[28–30] and ultracapacitor devices[31,32] has been demonstrated. Recently, there has been a growing interest in the incorporation of graphene into different kinds of advanced memory devices.[31–36] Indeed,

[a]Graduate Institute of Electronics Engineering, National Taiwan University, Taipei 106, Taiwan
[b]Department of Chemistry, National Taiwan Normal University, Taipei 116, Taiwan
[c]Department of Physics, National Sun Yat-Sen University, Kaohsiung 804, Taiwan
[d]Institute of Physics, National Chiao Tung University, Hsinchu 300, Taiwan
[e]Institute of Optoelectronic Sciences, National Taiwan Ocean University, Keelung 202, Taiwan
[f]Center for Emerging Material and Advanced Devices, National Taiwan University, Taipei 106, Taiwan
[g]Institute of Atomic and Molecular Sciences, Academia Sinica, Taipei 106, Taiwan
[h]Department of Materials Science and Engineering, National United University, Miaoli 360, Taiwan
[i]Department of Physics, National Taiwan University, Taipei 106, Taiwan. E-mail: yfchen@phys.ntu.edu.tw

† Electronic supplementary information (ESI) available: performance of devices with various GNF concentrations. See DOI: 10.1039/c2tc00010e

This journal is © The Royal Society of Chemistry 2013

Published on 30 October 2012. Downloaded by National Chiao Tung University on 28/04/2014 02:09:19.

organic bistable devices based on chemical vapor deposited (CVD) graphene[37] have exhibited good performances. However, the CVD technique requires the use of high temperature (850–1000 °C) and subsequent chemical treatment for transferring the graphene sheet once it has been grown. From an engineering perspective, this fabrication procedure is relatively time consuming and has a low throughput, particularly in the fabrication of multi-stack layer structures for 3D high-density storage arrays. In contrast to the CVD method, the most common approach to obtaining graphene-like materials is to chemically oxidize graphite before exfoliating the oxidized graphite in the liquid phase to form a graphene oxide solution.[38] For some applications, the obtained graphene oxide material still requires further functionalization[39–42] or toxic chemical and thermal treatment for obtaining its reduced state before it can be used.[43–46] Lotya *et al.*[47] reported a new method of producing graphene in flake form from exfoliated graphite in water–surfactant solutions. The obtained graphene flakes were submicron in size (graphene nanoflakes, GNFs), formed in the reduced state, and suspended in the liquid phase. These unique features promote graphene for use in more diverse applications using one-step simple low-temperature processing methods. The application of the GNF solution has initially been realized by our group in organic solar cells[48] as electron collection spots.

In the further exploration of the potential of graphene in macromolecular memory devices with simple and low-cost manufacturing processes, a GNF solution derived directly from graphite is an alternative option to approach the goal. Herein, we provide a promising method for the integration of graphene into macromolecular memory devices by a remarkably simple one-step solution process, eliminating any high temperature, material transfer, and chemical treatment processes. We demonstrate a macromolecular memory device based on a composite film of exfoliated GNFs blended with poly(vinyl alcohol) (PVA) and use a configuration of ITO/GNF–PVA/Ag to show bistable electrical switching behavior and nonvolatile rewritable memory effects under ambient conditions. The device exhibits an excellent performance including low power switch voltages, a long retention time, and high stability. In order to understand the underlying working principle of the newly designed GNF–PVA memory devices, carrier transport and switching mechanisms are proposed and discussed. It is worth emphasizing that the materials of the active layer are devised with a completely non-harmful solvent (water), which is very useful for fabricating nontoxic and eco-friendly organic devices. Furthermore, the material used in our devices is a highly flexible polymer, which also offers great potential for flexible electronic applications.

Experimental details

Materials

Graphite powder was purchased from Sigma-Aldrich Co. (product number 332461) and used after sieving through a 0.5 mm mesh. Sodium dodecylbenzenesulfonate (SDBS) was purchased from Sigma-Aldrich Co. (product number 289957) and used as received. Insulating poly(vinyl alcohol) (PVA) with a molecular weight of approximately 205 000 g mol^{-1} was purchased from Sigma-Aldrich Co. (product number 324590) and used without further purification.

Preparation of the liquid phase of graphene nanoflakes (GNFs)

The liquid phase of graphene was prepared by the exfoliation of graphite in a surfactant–water solution according to the literature.[47] A solution of SDBS surfactant of concentration 10 mg ml^{-1} was prepared in deionized (DI) water by stirring overnight. The surfactant was known to stabilize dispersions of graphene nanoflakes. A 10 mg portion of graphite powder and 15 ml of the desired SDBS concentration were mixed together in cylindrical vials. The mixture was then subjected to ultrasonication for 30 min in an ultrasonic bath (Branson ultrasonicator). The resulting dispersions were left to stand for one day to allow unstable aggregates to form and precipitate, and then centrifuged at 500 rpm for 90 min. After centrifugation, the top 75% of the dispersion in the vials was carefully removed using a pipette and stored until needed for further experimentation. Before use, the liquid phase of the graphene nanoflakes was sonicated for 20 min and used after passing through a 0.22 mm filter. This procedure produced dispersed graphene nanoflakes in water at loadings of ~4.6 mg ml^{-1}.

Preparation of a solution of GNF–PVA composite

To fabricate the GNFs blended with PVA as an active layer, we added 120 mg of PVA to 4 ml of the liquid phase of graphene. Then, the GNF–PVA mixture was stirred at 60 °C for one day. The PVA might have acted as a charge blocking material in the composite and provided good adhesion to the substrate. It was difficult for mixtures containing less than 13.3% of GNFs to show rewritable memory characteristics (ESI, Fig. S1†).

Device fabrication

A graphene-based macromolecular memory device was fabricated on an indium–tin-oxide (ITO) coated glass (~15 Ω sq^{-1}) substrate using the thin-film solution-process technique. Before the deposition of the active layer, the ITO glass was pre-cleaned sequentially with deionized water, acetone, and 2-propanol by ultrasonication, for 15 min each. The as-prepared aqueous solution of the GNF–PVA composite was spin-coated onto the ITO substrate at 4000 rpm for 60 s, followed by curing on a hot plate at 180 °C in air for 10 min to remove the residual solvent. The thickness of the active layer was about 150 nm. Finally, silver electrodes about 100 nm thick were thermally evaporated at a pressure of 6×10^{-7} Torr with a uniform deposition rate of 2 Å s^{-1}. The typical active area for the bistable memory device was 3 mm^2.

Characterization

Electrical characterization of the bistable electrical device was carried out using an Agilent 4156C semiconductor parameter analyzer equipped with an Agilent 41501B. All of the electrical properties were characterized at room temperature under

Published on 30 October 2012. Downloaded by National Chiao Tung University on 28/04/2014 02:09:19.

ambient conditions. Transmission electron microscopy (TEM) observations were performed using a Philips Technai G2 FEI-TEM system. μ-Raman scattering spectra were measured by a Jobin-Yvon T64000 system. A cross-sectional scanning electron microscope (SEM) image was observed using a JEOL JSM-6500F system.

Results and discussion

Fig. 1(a) shows a schematic diagram of the fabrication process for the GNF–PVA macromolecular composite memories. The device possessed a simple structure with the GNF–PVA composite as the active layer sandwiched between the indium–tin-oxide (ITO) and silver (Ag) electrodes. The liquid phase of the GNFs was prepared by the exfoliation of graphite according to a previous report[47] and the resulting solution was characterized using transmission electron microscopy (TEM) and Raman scattering spectroscopy. Fig. 1(b) and (c) demonstrate the typical TEM image and Raman scattering spectrum of the GNFs in the as-prepared suspension solution, respectively. After spin-coating the GNF–PVA solution onto the ITO-coated glass, an Ag layer was then thermally deposited on top of the active layer to complete the device fabrication as shown by the cross-sectional image of the device recorded using FESEM (field emission SEM) shown in Fig. 1(d). The typical thickness of the active layer was about 150 nm.

To characterize the electrical bistable switching behavior of the device, a voltage bias was applied to the Ag electrode with an appropriate current compliance of 0.001 A to prevent the device from hard breakdown, and the ITO electrode was used as the reference electrode. All electrical measurements were performed under ambient conditions. The electrical properties and memory effects of the ITO/GNF–PVA/Ag sandwich structure are illustrated by the DC current–voltage (I–V) characteristics. Fig. 2(a) and (b) show semi-logarithmic plots of the I–V curves for the positive- and negative-bias regimes, respectively. The arrows denote the sweeping direction of the voltage. During the first sweep from 0 to +2.5 V (Fig. 2(a), sweep 1), the device

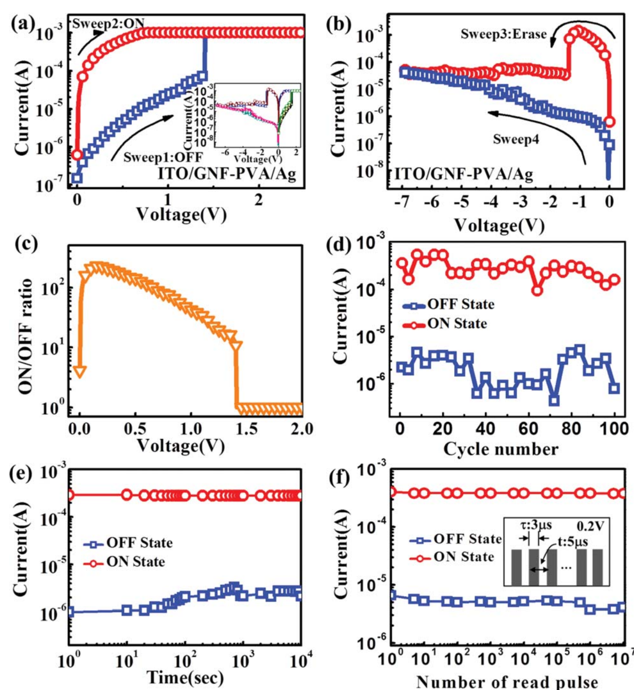

Fig. 2 Electrical properties of the ITO/GNF–PVA/Ag device. (a) Semi-logarithmic plots of the I–V curve for the positive-region with an appropriate current compliance. The inset shows the measurements in successive sweeps. (b) Semi-logarithmic plots of the I–V curve for the negative-region. (c) The ON/OFF ratio as a function of applied bias in the positive-region. (d) Reading of the current of the ON/OFF states at a reading voltage of +0.2 V over 100 switch cycles. (e) Data retention ability of the programmed ON/OFF state at +0.2 V. (f) Effect of a succession of pulses at a reading bias of +0.2 V on the device current in the written ON/OFF state. The inset shows the pulses used for the measurements.

current increased monotonically with the applied bias up to +1.4 V, followed by an abrupt increase in the current flow. This high current state remained as the applied voltage increased further. This high conductivity state was also confirmed by the second sweep from 0 to +2.5 V (Fig. 2(a), sweep 2) showing a good stability feature even after the power had been turned off. The device underwent a transition from the low-current (OFF-state) to a high-current state (ON-state) at a turn-on voltage of +1.4 V and this one-way conductance switching behavior is equivalent to the "writing" command in the memory device. Subsequent voltage scans in the negative-bias regime returned the conductivity of the device to its initial state. After reading the ON-state in the negative bias (Fig. 2(b), sweep 3), a suitable negative bias could switch the ON-state back to the original OFF-state at a turn-off voltage of approximately −1.3 V. Once the device was turned-off, no conductivity transition occurred during the following voltage sweep from 0 to −7 V (Fig. 2(b), sweep 4). This ON- to OFF-state switching process was able to erase the data stored in the ON-state. The OFF-state of the device could be rewritten to the ON-state by the application of a suitable bias. Such write/erase processes were repeated cyclically in successive sweeps and we obtained similar threshold voltages and asymmetric switching I–V curves (see the inset in Fig. 2(a)). Fig. 2(c) shows the ON-to-OFF state current ratio as a function of the applied voltage. The maximum

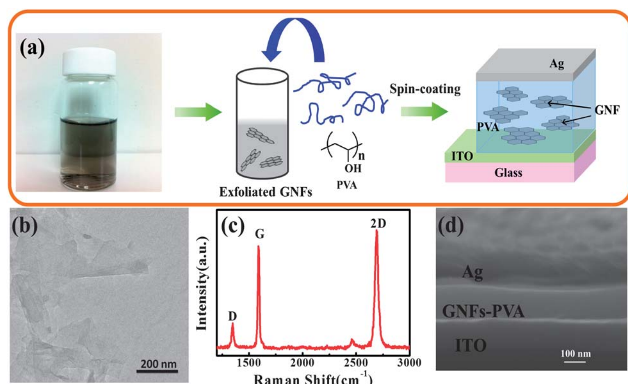

Fig. 1 (a) Schematic diagram for the fabrication process of a GNF–PVA based composite macromolecular memory device. (b) Transmission electron microscope (TEM) image of the as-prepared graphene nanoflakes. (c) Raman scattering spectrum of the as-prepared graphene nanoflakes. (d) Cross-sectional scanning electron microscope (SEM) image of the device.

 This journal is © The Royal Society of Chemistry 2013

Published on 30 October 2012. Downloaded by National Chiao Tung University on 28/04/2014 02:09:19.

ON/OFF current ratio was approximately 10^2 at a reading voltage of +0.2 V, which is readily distinguishable in memory applications. We then performed cycle tests on the device by performing the write/erase operation 100 times (Fig. 2(d)) and the current values at +0.2 V were read every four switches. The ON/OFF current ratio was still maintained after 100 switch cycles. A fluctuation in the ON- and OFF-states was expected after a series of switches. This can be explained by the fact that continuous device operation might induce lots of defects in the polymer layer, which is known as stress-induced leakage current,[49] and the electrical properties of the device might be affected by the absorption of air and moisture.[50] Thus, the presented ITO/GNF–PVA/Ag device exhibited a typical bistable electrical switching and rewritable nonvolatile memory effect with low ON- and OFF-switching voltages. When we changed the top electrode to Al or Pt, there was no noticeable switching behavior of the devices, implying that the Ag electrode used might be involved in the conductivity modulation.

In addition to the low turn-on/off voltages, data retention and pulse voltage stresses are also important parameters for memory devices. To test the data retention ability, the ON/OFF state was recorded at regular intervals at a reading voltage of +0.2 V. As shown in Fig. 2(e), the programmed ON and OFF states were maintained at the same order of magnitude without significant degradation for a considerable duration of 10^4 s. This excellent electrical stability achieved without applying a constant stress voltage is good for application in nonvolatile memory devices. For exploring the effect of the pulse voltage stress, the written data was read out under a succession of pulse reading biases of +0.2 V with a pulse duration of 3 μs and a repetition period of 5 μs. As shown in Fig. 2(f), the stored information was fairly stable when read up to 10^7 times. From a

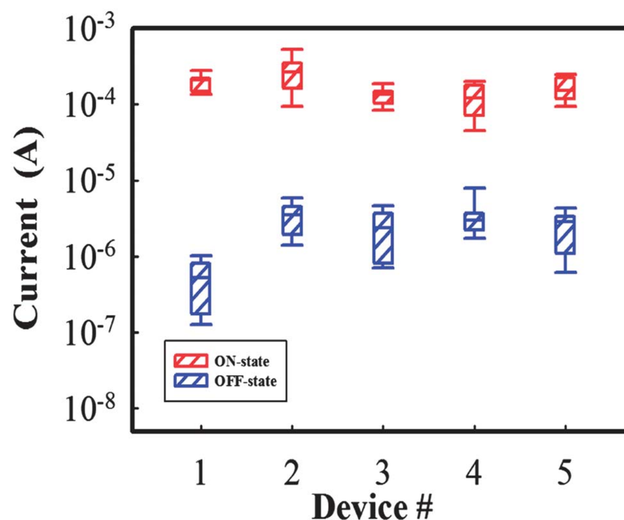

Fig. 3 Cell-to-cell variations of ON- and OFF-state currents for the devices.

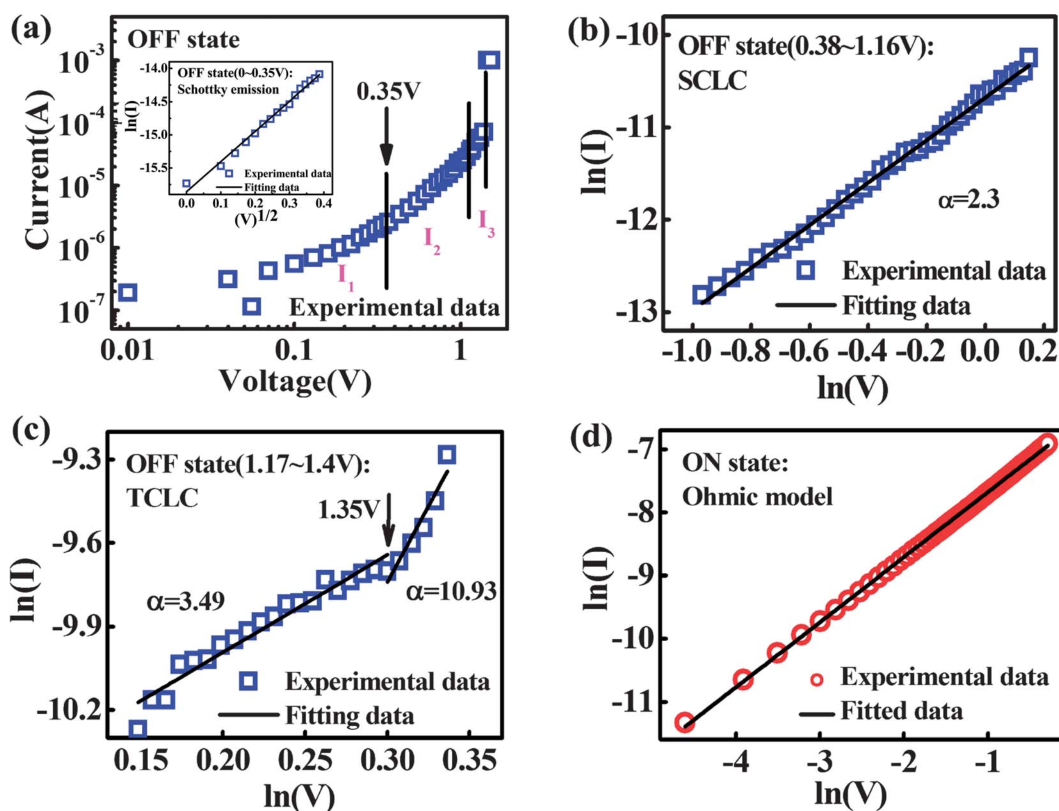

Fig. 4 Experimental data and theoretical fitting results for *I*–*V* curves for the ITO/GNF–PVA/Ag devices. (a) Logarithmic plots of *I versus V* for the OFF-state divided into three distinct regions I_1–I_3. The inset shows the fitted results in the low bias region I_1 using the Schottky emission model. (b) Region I_2 for the SCLC model. (c) Region I_3 for the trap-limited SCLC model. (d) The ON-state current can be fitted by the Ohmic model.

Published on 30 October 2012. Downloaded by National Chiao Tung University on 28/04/2014 02:09:19.

device operation perspective, the stable performance features of the GNF–PVA composite might result in potential uses in a broad variety of storage applications, for example portable disks, low-cost electrical labels, and radio frequency identification (RFID) tags.

According to our observations, the switching behaviors of the devices failed suddenly after more than several hundred cycles. This might be attributed to multi-filament formation in the devices, which causes the filaments to be ruptured. Thus, the fatigue in our devices is a step function of switching cycles. For the cell-to-cell distribution of the device performance, we randomly selected 8 devices for testing and 5 of them exhibited similar results as shown in Fig. 3. The results show a slight fluctuation in the OFF-state currents while the ON-state currents are similar to each other. For previously reported devices, several methods have been proposed to obtain uniformity of device performance. For example, Cho *et al.*[51] used a semiconducting polymer as the matrix material and Kim *et al.*[52] used a scalable *via*-hole structure. In the present work, we provide a facile and promising strategy by doping the insulating polymer with solution phase GNFs for memory applications with the advantages of low-temperature, low-cost and rapid-manufacturing by a simple one-step solution-process.

To understand the working principle of the bistable effect based on the GNF–PVA functional composite described above, we analyzed *I*–*V* curves with appropriate charge transport models. For current in the OFF-state, the log–log plot of *I versus* *V* can be divided into three distinct regions (I_1–I_3), as shown in Fig. 4(a). In region I_1 ($V < +0.37$ V), the $I(V)$ curve can be fitted by the Schottky emission (SE) model; *i.e.*, thermionic emission[53] (see the inset in Fig. 4(a)):

$$I \propto AT^2 \exp\left[-\frac{\phi_B - q\sqrt{qV/4\pi\varepsilon d}}{kT}\right], \quad (1)$$

where A, T, k, ϕ_B, q, d, and ε are the Richardson constant, temperature, Boltzmann constant, Schottky energy barrier, electron charge, thickness of the film, and electric constant, respectively. The SE model suggests that the charge carriers from the electrodes can be injected into the composite after overcoming the hetero-material interface energy barriers. As the bias increases from +0.37 V to the threshold voltage, the current in regions I_2 and I_3 can be described by a space charge limited current (SCLC) model with trapping,[53] in which the *I*–*V* characteristics follow the expression:

$$I \propto V^{\alpha}, \quad (2)$$

As shown in Fig. 4(b) and (c), the slopes of the fits yield 2.3, 3.49 and 10.93. This result indicates that a typical trap-limited SCLC; *i.e.*, trapped charge-limit-current (TCSC) transport, dominated the electrical properties in the OFF-state for $\alpha > 2$. Son *et al.*[37] suggested that the region in which $\alpha \gg 2$ correlates with the exponential distribution of trap states within the insulator band gap. In the present GNF–PVA composite film, the conductive GNFs presumably acted as carrier traps.[54] This argument was also supported experimentally by the result that the device without GNFs showed no significant bistable behavior. Thus, GNFs play an important role in producing the memory effects. Similar phenomena have been reported in other hybrid organic–inorganic macromolecule memories, in which inorganic nanoparticles play a role as charge trapping and detrapping centers.[16,55] The current in the ON-state was fitted well by the Ohmic current model[53] (Fig. 4(d)):

$$I \propto V \exp\left(-\frac{\Delta E_{ae}}{kT}\right), \quad (3)$$

where ΔE_{ae}, T, and k are the activation energy, temperature, and Boltzmann constant, respectively. The slope for the fit yields 1.02, a result of the Ohmic conduction mechanism governing the ON-state carrier transport. It has been proposed that the Ohmic conduction in the ON-state of a memory device can be attributed to the metal filament model.[37,56] Cho *et al.*[51] directly observed the formation and dissolution of Ag bridges within the polymer film of memory cells. When a positive voltage is applied to the top Ag electrode, the electrochemically active Ag electrode might be oxidized by the reaction Ag → Ag^+ + e^-. The mobile Ag^+ cations diffuse toward the bottom electrode through the organic film and are reduced there by the injected electron flow. The Ag metal starts to grow from the bottom electrode and eventually reaches the top Ag electrode forming an Ag bridge to conduct electricity. In the present system, Ag^+ cations migrate through the PVA–GNF composite film to form conducting bridges between the top Ag and the bottom ITO electrodes.

The Ag filament formation can be further validated by area dependence and temperature dependence experiments. As

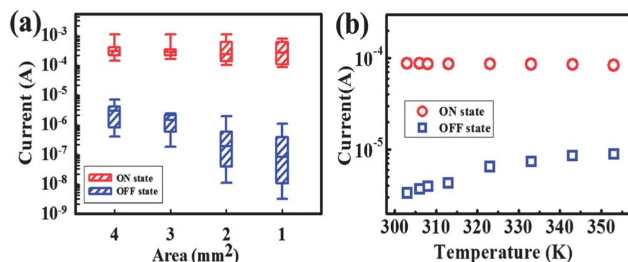

Fig. 5 (a) Current *versus* device area plot for the ON- and OFF-states. (b) Temperature dependence of the ON- and OFF-states.

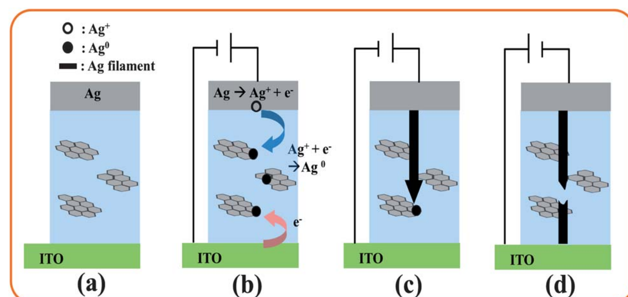

Fig. 6 Schematic concept of the switching mechanism for an ITO/GNF–PVA/Ag memory device. (a) Device structure. (b) Charge capture by the GNFs and ionization, reduction, and drift processes of silver ions caused by a positive voltage. (c) Metal filament formation. (d) The rupture of the metal filament by Joule heating.

This journal is © The Royal Society of Chemistry 2013

Published on 30 October 2012. Downloaded by National Chiao Tung University on 28/04/2014 02:09:19.

shown in Fig. 5(a), there was no significant difference in the ON-state current level among devices with various areas; *i.e.*, 1, 2, 3, and 4 mm^2 This could be attributed to local conductive path formation in a small area due to the electrochemical redox reaction of the top Ag electrode. Thus, the ON-state current flow weakly depends on the electrode area. Further evidence can be obtained by the temperature dependency of the ON-state current. As shown in Fig. 5(b), the ON-state current level is slightly affected by the temperature within the window measured while the OFF-state current value increases with an increasing temperature. The temperature independent behavior of the ON-state current flow indicates that the charge movement in the active channel is not through hopping in contrast to the thermal energy assisted hopping behavior in the OFF-state. The weak area-dependence and temperature-insensitivity of the ON-state current flow are also the indirect evidence for local conducting filament formation in the active layer.[52]

Based on the analysis and results described above, the charge transport in the GNF–PVA composite film involved charge trapping and local metal filament forming processes. The working principle of the GNF–PVA memory device can therefore be understood as follows. Fig. 6(a) and (b) illustrate the switching mechanism for the bistable effect based on the GNF–PVA composite film. In general, the insulating PVA acted as a charge blocking medium in the composite. The work function of the GNFs determined by ambient photoelectron spectroscopy (Riken-Keiki AC-2) is −5.0 eV, which is comparable to ∼−4.6 eV for chemical vapor deposited (CVD) graphene.[57] The GNFs with a high work function (−5.0 eV) dispersed randomly in the insulating PVA layer might act as electron traps to capture electrons injected from electrodes. Initially, for $V \leq +0.35$ V, electrons from the ITO electrode would be injected into the active layer after overcoming the interfacial barrier. As $V > +0.35$ V, the number of injected electrons followed a typical SCLC model with trapping (TCLC) and a large amount of charge was subsequently captured by the GNFs as the applied bias increased (Fig. 6(b)). Meanwhile, the Ag^+ that underwent dissolution from the Ag electrode can be driven into the composite and reduced there by receiving trapped electrons from the GNFs or ITO electrode (Fig. 6(b)). When the applied bias reaches the turn-on voltage, an Ag conducting filament is formed within the PVA–GNF film, resulting in an abrupt increase in the current and leading to an OFF- to ON-state transition (Fig. 6(c)). This metal filament can be preserved even in the absence of an external applied voltage, which suggests that it is nonvolatile in nature. Consequently, the device can exhibit a "writing" operation, in which it is switched from the low-conductivity (OFF) to the high-conductivity (ON) state. By applying a negative bias of approximately −1.3 V to the ON-state device, the Joule heating effect caused by the high current flow might annihilate the conducting filament after the current has passed through it. After the rupture of the filament, the device can be switched back to the OFF-state (Fig. 6(d)).

We emphasize here that the bistable memory characteristics of the PVA–GNF cells were observed when the initial voltage sweep started from the positive bias quadrant. Upon reversing the initial bias sweeping direction, there was no significant change in the conductance within the applied voltage window. Such asymmetric electrical switch behaviors are widely explained by the formation and rupture of a local conducting filament with the assistance of electrochemically active electrode reactions.[3,58] In addition, the device without GNFs showed no significant bistable characteristics. Therefore, based on the above observations, the electrochemical reaction of Ag material and the presence of GNFs are important in the low voltage switching operation. The relatively low switching voltage in our system may be attributed to the existence of charged GNFs in the PVA polymer, which can rapidly supply electrons to neutralize Ag^+ before it reaches the bottom ITO electrode. Compared to tri-layer devices using a CVD graphene sheet, our device exhibited lower operation voltages and excellent properties, such as good retention time and good stability. In contrast to other emerging memory work, such as that on phase-change and charge trapping memory, redox-based resistive switching memory devices are expected to have the merits of low energy operation, high-density, fast writing and low cost.[3,58] Most importantly, our strategy provides a promising approach for the generation of graphene-based macromolecular memory devices with the advantages of low-temperature operation, large-area and rapid-manufacturing by a simple one-step solution-process.

Conclusions

In summary, a liquid phase of exfoliated graphene nanoflakes produced using a facile method has been successfully used to fabricate GNF–PVA nonvolatile macromolecular memory devices for the first time by a simple solution-process. The devices presented exhibited excellent bistable electrical switching behaviors and nonvolatile rewritable memory effects under ambient conditions, with low turn-on and turn-off voltages of about +1.4 V and −1.3 V, respectively. The maximum ON/OFF ratio is greater than 100, which is readily distinguishable in memory applications. In addition, both the written ON and OFF states were stable for over 10^4 s without significant degradation, and the programmed states could endure up to 10^7 reading cycles under a pulse reading voltage of +0.2 V. The stable performance of the graphene-based composite macromolecular memory devices suggests promising application potentials in a wide variety of commercial products. The carrier transport mechanism of the GNF–PVA composite film was resolved by the analysis of *I–V* curves. The results showed that the device followed the typical trap-limited SCLC model (TCLC) in the OFF-state and the Ohmic law in the ON-state. The electrical switch behavior with a low bias was attributed to the electrochemical reaction of the Ag material within the composite film assisted by charged GNFs. Finally, it is stressed here that our approach provides a promising method for the fabrication of graphene-based macromolecular memory devices with high performances by a significantly simple solution-process, and includes the advantages of low-cost, large-area and rapid-manufacturing for next-generation memory devices. In addition, with the eco-friendly and highly flexible materials used in our devices, our study should be very useful and timely.

Published on 30 October 2012. Downloaded by National Chiao Tung University on 28/04/2014 02:09:19.

Acknowledgements

This work was supported by the National Science Council and the Ministry of Education of the Republic of China.

Notes and references

1 B. Park, B. Kang, S. Bu, T. Noh, J. Lee and W. Jo, *Nature*, 1999, **401**, 682–684.
2 M. Wuttig and N. Yamada, *Nat. Mater.*, 2007, **6**, 824–832.
3 R. Waser and M. Aono, *Nat. Mater.*, 2007, **6**, 833–840.
4 M. Baibich, J. Broto, A. Fert, F. N. Van Dau, F. Petroff, P. Etienne, G. Creuzet, A. Friederich and J. Chazelas, *Phys. Rev. Lett.*, 1988, **61**, 2472–2475.
5 J. Ouyang, C. W. Chu, C. R. Szmanda, L. Ma and Y. Yang, *Nat. Mater.*, 2004, **3**, 918–922.
6 L. Ma, J. Liu and Y. Yang, *Appl. Phys. Lett.*, 2002, **80**, 2997–2999.
7 T. W. Kim, Y. Yang, F. Li and W. L. Kwan, *NPG Asia Mater.*, 2012, **4**, e18, DOI: 10.1038/am.2012.32.
8 Y. Yang, J. Ouyang, L. Ma, R. J. H. Tseng and C. W. Chu, *Adv. Funct. Mater.*, 2006, **16**, 1001–1014.
9 B. Cho, S. Song, Y. Ji, T. W. Kim and T. Lee, *Adv. Funct. Mater.*, 2011, **21**, 2806–2829.
10 Q. D. Ling, F. C. Chang, Y. Song, C. X. Zhu, D. J. Liaw, D. S. H. Chan, E. T. Kang and K. G. Neoh, *J. Am. Chem. Soc.*, 2006, **128**, 8732–8733.
11 S. G. Hahm, S. Choi, S. H. Hong, T. J. Lee, S. Park, D. M. Kim, W. S. Kwon, K. Kim, O. Kim and M. Ree, *Adv. Funct. Mater.*, 2008, **18**, 3276–3282.
12 C. L. Liu and W. C. Chen, *Polym. Chem.*, 2011, **2**, 2169–2174.
13 C. W. Chu, J. Ouyang, J. H. Tseng and Y. Yang, *Adv. Mater.*, 2005, **17**, 1440–1443.
14 R. J. Tseng, J. Huang, J. Ouyang, R. B. Kaner and Y. Yang, *Nano Lett.*, 2005, **5**, 1077–1080.
15 J. C. Scott and L. D. Bozano, *Adv. Mater.*, 2007, **19**, 1452–1463.
16 J. Ouyang, C. W. Chu, C. R. Szmanda, L. Ma and Y. Yang, *Nat. Mater.*, 2004, **3**, 918–922.
17 A. K. Geim and K. S. Novoselov, *Nat. Mater.*, 2007, **6**, 183–191.
18 S. Stankovich, D. A. Dikin, R. D. Piner, K. A. Kohlhaas, A. Kleinhammes, Y. Jia, Y. Wu, S. T. Nguyen and R. S. Ruoff, *Carbon*, 2007, **45**, 1558–1565.
19 D. A. Dikin, S. Stankovich, E. J. Zimney, R. D. Piner, G. H. B. Dommett, G. Evmenenko, S. T. Nguyen and R. S. Ruoff, *Nature*, 2007, **448**, 457–460.
20 M. Y. Han, B. Ozyilmaz, Y. B. Zhang and P. Kim, *Phys. Rev. Lett.*, 2007, **98**, 206805.
21 K. S. Kim, Y. Zhao, H. Jang, S. Y. Lee, J. M. Kim, J. H. Ahn, P. Kim, J. Y. Choi and B. H. Hong, *Nature*, 2009, **457**, 706–710.
22 C. Lee, X. D. Wei, J. W. Kysar and J. Hone, *Science*, 2008, **321**, 385–388.
23 D. Abergel, V. Apalkov, J. Berashevich, K. Ziegler and T. Chakraborty, *Adv. Phys.*, 2010, **59**, 261–482.
24 E. Hill, A. Vijayaraghavan and K. Novoselov, *IEEE Sensor J.*, 2011, **11**, 3161–3170.
25 J. Bai, X. Zhong, S. Jiang, Y. Huang and X. Duan, *Nat. Nanotechnol.*, 2010, **5**, 190–194.
26 B. J. Kim, H. Jang, S. K. Lee, B. H. Hong, J. H. Ahn and J. H. Cho, *Nano Lett.*, 2010, **10**, 3464–3466.
27 X. Yang, G. Liu, A. A. Balandin and K. Mohanram, *ACS Nano*, 2010, **4**, 5532–5538.
28 Z. Liu, J. Li, Z. H. Sun, G. Tai, S. P. Lau and F. Yan, *ACS Nano*, 2011, **6**, 810–818.
29 S. S. Li, K. H. Tu, C. C. Lin, C. W. Chen and M. Chhowalla, *ACS Nano*, 2010, **4**, 3169–3174.
30 Y. Y. Lee, K. H. Tu, C. C. Yu, S. S. Li, J. Y. Hwang, C. C. Lin, K. H. Chen, L. C. Chen, H. L. Chen and C. W. Chen, *ACS Nano*, 2011, **5**, 6564–6570.
31 O. O. Ekiz, M. Urel, H. Guner, A. K. Mizrak and A. Dana, *ACS Nano*, 2011, **5**, 2475–2482.
32 A. Sinitskii, A. Dimiev, D. V. Kosynkin and J. M. Tour, *ACS Nano*, 2010, **4**, 5405–5413.
33 T. J. Echtermeyer, M. C. Lemme, M. Baus, B. N. Szafranek, A. K. Geim and H. Kurz, *IEEE Electron Device Lett.*, 2008, **29**, 952–954.
34 B. Standley, W. Bao, H. Zhang, J. Bruck, C. N. Lau and M. Bockrath, *Nano Lett.*, 2008, **8**, 3345–3349.
35 A. J. Hong, E. B. Song, H. S. Yu, M. J. Allen, J. Kim, J. D. Fowler, J. K. Wassei, Y. Park, Y. Wang, J. Zou, R. B. Kaner, B. H. Weiller and K. L. Wang, *ACS Nano*, 2011, **5**, 7812–7817.
36 H. Y. Jeong, J. Y. Kim, J. W. Kim, J. O. Hwang, J. -E. Kim, J. Y. Lee, T. H. Yoon, B. J. Cho, S. O. Kim, R. S. Ruoff and S. -Y. Choi, *Nano Lett.*, 2010, **10**, 4381–4386.
37 D. I. Son, T. W. Kim, J. H. Shim, J. H. Jung, D. U. Lee, J. M. Lee, W. I. Park and W. K. Choi, *Nano Lett.*, 2010, **10**, 2441–2447.
38 W. S. Hummers Jr and R. E. Offeman, *J. Am. Chem. Soc.*, 1958, **80**, 1339.
39 G. Liu, X. Zhuang, Y. Chen, B. Zhang, J. Zhu, C. X. Zhu, K. G. Neoh and E. T. Kang, *Appl. Phys. Lett.*, 2009, **95**, 253301.
40 X. D. Zhuang, Y. Chen, G. Liu, P. P. Li, C. X. Zhu, E. T. Kang, K. G. Noeh, B. Zhang, J. H. Zhu and Y. X. Li, *Adv. Mater.*, 2010, **22**, 1731–1735.
41 P. Cui, S. Seo, J. Lee, L. Wang, E. Lee, M. Min and H. Lee, *ACS Nano*, 2011, **5**, 6826–6833.
42 B. Zhang, Y. L. Liu, Y. Chen, K. G. Neoh, Y. X. Li, C. X. Zhu, E. S. Tok and E. T. Kang, *Chem.–Eur. J.*, 2011, **17**, 10304–10311.
43 J. Q. Liu, Z. Y. Yin, X. H. Cao, F. Zhao, A. P. Lin, L. H. Xie, Q. L. Fan, F. Boey, H. Zhang and W. Huang, *ACS Nano*, 2010, **4**, 3987–3992.
44 G. Eda, C. Mattevi, H. Yamaguchi, H. K. Kim and M. Chhowalla, *J. Phys. Chem. C*, 2009, **113**, 15768–15771.
45 G. Eda, G. Fanchini and M. Chhowalla, *Nat. Nanotechnol.*, 2008, **3**, 270–274.
46 J. Q. Liu, Z. Q. Lin, T. J. Liu, Z. Y. Yin, X. Z. Zhou, S. F. Chen, L. H. Xie, F. Boey, H. Zhang and W. Huang, *Small*, 2010, **6**, 1536–1542.
47 M. Lotya, Y. Hernandez, P. J. King, R. J. Smith, V. Nicolosi, L. S. Karlsson, F. M. Blighe, S. De, Z. Wang and I. McGovern, *J. Am. Chem. Soc.*, 2009, **131**, 3611–3620.

This journal is © The Royal Society of Chemistry 2013

48 Y. M. Sung, F. C. Hsu, D. Y. Wang, I. S. Wang, C. C. Chen, H. C. Liao, W. F. Su and Y. F. Chen, *J. Mater. Chem.*, 2011, **21**, 17462–17467.
49 S. Choi, S. H. Hong, S. H. Cho, S. Park, S. M. Park, O. Kim and M. Ree, *Adv. Mater*, 2008, **20**, 1766–1771.
50 Q. D. Ling, D. J. Liaw, C. Zhu, D. S. H. Chan, E. T. Kang and K. G. Neoh, *Prog. Polym. Sci.*, 2008, **33**, 917–978.
51 B. Cho, J. M. Yun, S. Song, Y. Ji, D. Y. Kim and T. Lee, *Adv. Funct. Mater*, 2011, **21**, 3976–3981.
52 T. W. Kim, H. Choi, S. H. Oh, M. Jo, G. Wang, B. Cho, D. Y. Kim, H. Hwang and T. Lee, *Nanotechnology*, 2009, **20**, 025201.
53 S. M. Sze, in *Physics of Semiconductor Devices*, Wiley, New York, 2nd edn, 1981, p. xii, p. 868.
54 A. H. C. Neto, F. Guinea, N. Peres, K. Novoselov and A. Geim, *Rev. Mod. Phys.*, 2009, **81**, 109–162.
55 D. I. Son, D. H. Park, W. K. Choi, S. H. Cho, W. T. Kim and T. W. Kim, *Nanotechnology*, 2009, **20**, 195203.
56 D. I. Son, J. H. Shim, D. H. Park, J. H. Jung, J. M. Lee, W. I. Park, T. W. Kim and W. K. Choi, *Nanotechnology*, 2011, **22**, 295203.
57 Y. J. Yu, Y. Zhao, S. Ryu, L. E. Brus, K. S. Kim and P. Kim, *Nano Lett.*, 2009, **9**, 3430–3434.
58 R. Waser, R. Dittmann, G. Staikov and K. Szot, *Adv. Mater.*, 2009, **21**, 2632–2663.

Published on 30 October 2012. Downloaded by National Chiao Tung University on 28/04/2014 02:09:19.